Aerated wave impacts on floating bodies

Martin van der Eijk,[1*] Peter R. Wellens,[1] Reinier W. Bos[1]
[1]Department of Marine and Transport Technology, University of Technology Delft, the Netherlands
[*]To whom correspondence should be addressed; E-mail: m.vandereijk@tudelft.nl.

Introduction

An estimated 10% of all structural damages of conventional ships is caused by slamming, breaking waves and green water (Wang et al., 2002). Water and air interact during these complex free surface events leading to entrained air in water. Finite volume methods are used to predict the behavior of the fluid in such cases, as well as the loads on floating structures operating in them. These methods are often based on a continous multifluid model with the assumption of incompressible water.
The benefit of modelling air entrainment is that the impact pressure is cushioned: it is smeared out over time decreasing its peaks. At the same air entrainment can cause pressure oscillations and sub-atmospheric pressures, causing positive and negative forces on the structure. Additionally the forces can increase in magnitude due to an extension of the area of impact due to cushioning (Bredmose et al., 2009; Bullock et al., 2007; Obhrai et al., 2005).

Here a dam break is investigated as a representative case for wave impact phenomena, especially for green water. The objective is to demonstrate with dam break simulations that oscillations in entrapped air pockets can cause pressure level variations of the order of the impact pressure. We choose to simulate in 2D, because of the increased likelihood of entrapping a pocket of air. The domain and initial conditions for the 3D experiment of MARIN are shown in Fig. 1. This case on model scale is still without the obstacle illustrated by the dashed square where for the next case on real scale an obstacle is imposed.

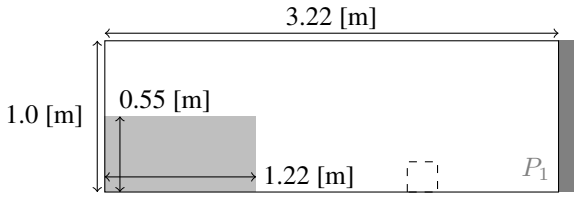

Figure 1: Setup 2D dam break at model scale. The object of the second test case is represented by the dashed lines.

Dam break

The dam break experiments were conducted as follows: the door was pulled up, releasing a dam of water with size $0.55[m]\times1.22[m]$. The water flows towards the opposite domain wall. There, an impact takes place with significant run-up and overturning, after which the disturbance propagates back and forth between the walls. The pressure P_1 is measured at the foot of the wall at a height of $0.03[m]$.

To model the experiment, an in-house code is used based on the multifluid models of T. Kleefsman (2005); Wemmenhove et al. (2015). The method uses a cut-cell method which has the benefit that only one grid is needed to represent the object and the flow, with a Cartesian grid. A second-order Adam-Bashforth time integration is used for the convective as well as the diffusive term, and a second-order upwind scheme for the convective term. The pressure is solved implicitly. The capillary forces are calculated using a continuum surface force model (Brackbill et al., 1992).

The interface is reconstructed using piecewise linear interface calculation. The mixture is advanced by (2) using a forward-Euler scheme. Together with a local height function and an improved labelling system based on the method described by K. Kleefsman et al. (2005), a sharp interface is maintained. For the cut-cells, a virtual cell-merging method is applied to prevent numerical pressure peaks. The simulation results are shown in Fig. 2.

Fig. 2a shows the measured and calculated pressure of the dam break. Besides the differences with the experimental results caused due to the extra third dimension, special attention goes out to the pressure oscillations at P_1 showed in the

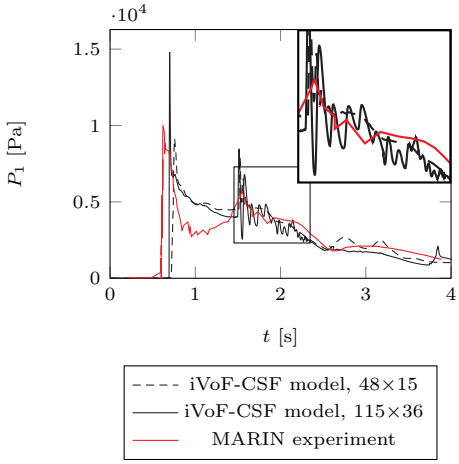

(a) Pressure at the foot

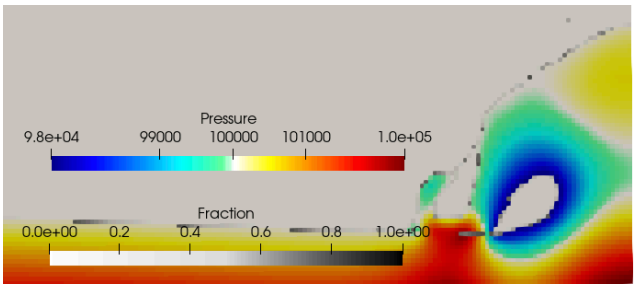

(b) Pressure snapshot at right domain wall with p_{atm} is $10^5[Pa]$

Figure 2: Pressure signal P_1

enlargement of Fig. 2a. These are due to the air pocket that is entrapped at around t=1.5[s] after the run-up on the domain wall has overturned. The air pocket is shown in Fig. 2b at time instance t=1.54[s] where the pressure in the air pocket is lower than the atmospheric pressure (p_{atm}) leading to a compression.

By averaging the pressure in the air pocket over space, a high frequency oscillation of 14.0[Hz] is found. The same characteristic high frequency oscillation is found for the pressure signal P_1 at the wall by applying a Fourier transform of the pressure signal between 1.2[s] and 2.4[s]. In P_1, also a low frequency of around 3.0[Hz] is found. This corresponds to the global motion of the air pocket in space. The higher frequency peaks than 14.0[Hz] were observed which are caused by breaking-up of the pocket or due to higher harmonics (Plumerault et al., 2012).

The current method can model the compressible effects of the air pocket showing that for this case the pressure oscillations are in the order of the impact pressure. However, for a real impact it is unlikely that there is just a single large air entrapment and no smaller bubbles.

Influence of bubble clouds

A closer look at such an impact like during the dam break shows how air is distributed over the water, as shown in Fig. 3b. There are air pockets spanning multiple cells, and bubble clouds which are smaller than one cell. Both of these effects change the compressibility of the water, but in the current multifluid model the bubble clouds are not taken into account becaue they are on a smaller resolution than the grid. To take the bubbles into account for modelling a floating body at real scale would require a grid resolution in the order of 10^{30} grid cells to reconstruct these bubble clouds (Castro et al., 2016).

In case of not reconstructing the bubble clouds and still taking into account the compressible effects, a homogeneous mixture of air and water is assumed by neglecting surface tension, interaction of bubbles and buoyancy effects. The compressibility of a mixture can be indicated with a Mach number, depending on the change of pressure over density for an isothermal flow (speed of sound, see Fig. 3a). The entrainment of a small amount of air drastically modifies the compressibility of the mixture up to several orders. The current method cannot represent these acoustic properties.

Besides the entrainment of air during the wave impact of interest, it already can contain bubble clouds before impact. Air can be entrained in the water for a previous breaking wave, but also for white capping waves and droplet impacts. These events can lead to impacts of compressible aerated waves on structures which makes the current method inadequate.

An extended model is discussed which can represent the right acoustic properties at the scale of bubble clouds for an isothermal flow. The computational costs of the method hardly increase due small changes in the system of equations.

Extended method

Here we extend our method to take into account the compressibility of water caused by bubbles smaller than the grid size. The mixture is still governed by the Navier-Stokes equations, with pressure equilibrium and no slip condition between the

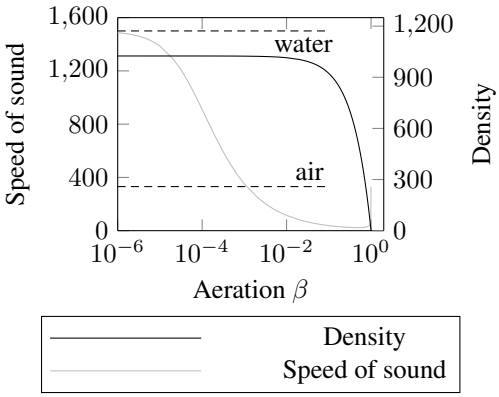

(a) Density & Speed of sound for mixture vs Bubble cloud fraction β (Wood, 1941).

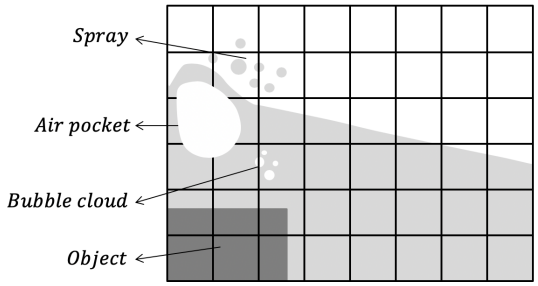

(b) Definition bubble cloud fraction β at subgrid level, air pocket fraction F_s at grid level and object fraction F_b.

Figure 3: The effect of aeration for numerical grids and properties.

fluids. Hence there is still one unique field for velocity and pressure, only the equation of state changes.

Differences are found in the definition of the density (ρ) where an extra volume fraction (β) is added indicating the volume fraction of bubble clouds.

$$\rho = \frac{F_s}{F_b}\rho_m + \frac{F_b - F_s}{F_b}\rho_a \text{ with } \rho_m = (1-\beta)\rho_w + \beta\rho_a, \tag{1}$$

where ρ is the density for air (a) or mixture (m). The volume fraction F_b indicates the volume which is not governed by the object, illustrated in Fig. 3b. The remaining volume can be filled by the mixture, indicated by the volume fraction F_s. The mixture may contain air with a volume fraction β.

Both fluids, water and air, are assumed barotropic. Assuming an isothermal flow, the following equation is derived

$$\frac{DF_s}{Dt} = (F_b - F_s)H\nabla \cdot \mathbf{u}, \tag{2}$$

where H is a function of the participation and the compressibility of air and water in a cell. The transport equation ensures pressure equilibrium under compression and expansion without heat transfer by a change in volume fraction F_s. To close the system again, for the liquid density an isothermal equation of state is used.

After updating the volume fraction field of the mixture, the aeration β is updated by assuming an initial mass fraction of air in water. Due to the homogeneous conditions, the mass fraction remains constant, capillary and buoyancy effects are neglected. A similar approach is used by Plumerault et al. (2012).

Dam break with aerated water

To capture the compressible effects of aeration when the bubble cloud cannot be represented by the grid cells, a β_0 and so a mass fraction is initiated. The domain in Fig. 1 is scaled with a factor of four to have a real scale. A squared obstacle is added at 9.56[m] positioned from the left domain wall with a size of 0.64[m], representing a (super)structure on deck.

The air fraction β_0 is likely to be in the order of one percent before impact (Peregrine & Thais, 1996). This results for this case in significant change of the speed of sound in Fig. 3a and so the Mach number. The results are shown in Fig. 4.
Until the first impact with the obstacle, the free surface dynamics is not affected by the aeration level. Hereafter, the force traces are different over time. The force by the first impact is cushioned non-linearly by an increase of β_0. Due to the difference in properties of the mixture, different oscillation frequencies and amplitudes are found in the pressure signals. A small difference in aeration can have major consequences on the results after the first impact.

The phenomenon found after 4.8[s] where the returning jet after impact with the wall hits the free surface is highlighted for the pressure at the foot of the wall (P_1) and the right side of the obstacle in Fig. 4c. An amplification of the pressure at the right side of the obstacle is found. This oscillation has a similar frequency as the longitudinal mode (f_l) between the obstacle and the wall which is function of the averaged aeration level and the distance between the obstacle and the wall. Due to the mixing of air and water behind the obstacle, a highly compressible mixture is found leading to slow-propagating compression waves. The compression waves are initiated between the obstacle and the wall through the mixture. This results in sub-atmospheric pressures at the obstacle as well as the wall.

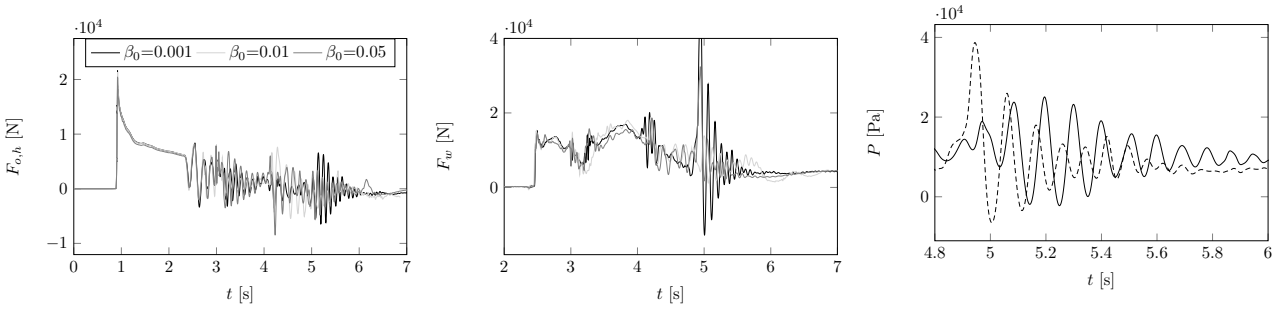

(a) Horizontal force on the obstacle

(b) Force on the wall

(c) Pressure at the foot of the wall (dashed) and obstacle (solid) for β_0=0.001.

Figure 4: Horizontal forces for different initial aeration level β_0

Conclusion

The importance of an air pocket for a dam break problem is illustrated: the entrapped air causes pressure oscillations having an amplitude of nearly the same size as the pressure of the initial impact. If the water is aerated, and therefore compressible, then the results are highly dependent on the aeration, even for very small volume fractions.

Further research efforts should be made to identify how a free surface event such as a breaking wave affects locally the volume fraction. For extreme wave impacts, the effect of air on every scale needs to be taken into account. This will lead to safer ships.

References

Brackbill, J., Kothe, D., & Zemach, C. (1992). A continuum method for modeling surface tension. *Journal of computational physics*, *100*(2), 335–354.

Bredmose, H., Peregrine, D., & Bullock, G. (2009). Violent breaking wave impacts. part 2: modelling the effect of air. *Journal of Fluid Mechanics*, *641*, 389–430.

Bullock, G., Obhrai, C., Peregrine, D., & Bredmose, H. (2007). Violent breaking wave impacts. part 1: Results from large-scale regular wave tests on vertical and sloping walls. *Coastal Engineering*, *54*(8), 602–617.

Castro, A. M., Li, J., & Carrica, P. M. (2016). A mechanistic model of bubble entrainment in turbulent free surface flows. *International Journal of Multiphase Flow*, *86*, 35–55.

Kleefsman, K., Fekken, G., Veldman, A., Iwanowski, B., & Buchner, B. (2005). A volume-of-fluid based simulation method for wave impact problems. *Journal of computational physics*, *206*(1), 363–393.

Kleefsman, T. (2005). Water impact loading on offshore structures. *A Numerical Study, EU Project No.: GRD1-2000-25656*.

Obhrai, C., Bullock, G., Wolters, G., Müller, G., Peregrine, H., Bredmose, H., & Grüne, J. (2005). Violent wave impacts on vertical and inclined walls: large scale model tests. In *Coastal engineering 2004: (in 4 volumes)* (pp. 4075–4086). World Scientific.

Peregrine, D., & Thais, L. (1996). The effect of entrained air in violent water wave impacts. *Journal of Fluid Mechanics*, *325*, 377–397.

Plumerault, L.-R., Astruc, D., Villedieu, P., & Maron, P. (2012). A numerical model for aerated-water wave breaking. *International Journal for Numerical Methods in Fluids*, *69*(12), 1851–1871.

Wang, G., Tang, S., Shin, Y., et al. (2002). A direct calculation approach for designing a ship-shaped fpso¿ s bow against wave slamming load. In *The twelfth international offshore and polar engineering conference.*

Wemmenhove, R., Luppes, R., Veldman, A., & Bunnik, T. (2015). Numerical simulation of hydrodynamic wave loading by a compressible two-phase flow method. *Computers & Fluids*, *114*, 218–231.

Wood, A. (1941). A textbook of sound, 578 pp. *Bell, London*.